Transient critical heat fluxes of subcooled water flow boiling in a SUS304-circular tube caused by a rapid decrease in velocity from non-boiling regime

Hata, Koichi

Fukuda, Katsuya

Masuzaki, Suguru

(Citation)
Experimental Thermal and Fluid Science,66:160-172

(Issue Date)
2015-09

(Resource Type)
journal article

(Version)
Accepted Manuscript

(URL)
https://hdl.handle.net/20.500.14094/90003473

TRANSIENT CRITICAL HEAT FLUXES OF SUBCOOLED WATER FLOW BOILING IN A SUS304-CIRCULAR TUBE CAUSED BY A RAPID DECREASE IN VELOCITY FROM NON-BOILING REGIME

Koichi Hata
Institute of Advanced Energy, Kyoto Univ., Gokasho, Uji, Kyoto 611-0011, Japan
Phone:+81-774-38-3473
hata@iae.kyoto-u.ac.jp

Katsuya Fukuda
Dept. of Marine Eng., Kobe Univ., 5-1-1, Fukaeminami, Kobe 658-0022, Japan
Phone: +81-75-753-3328
fukuda@maritime.kobe-u.ac.jp

Suguru Masuzaki
National Institute for Fusion Science, Oroshi-cho, Toki, Gifu 509-5292, Japan
Phone:+81-572-58-2168
masuzaki@lhd.nifs.ac.jp

ABSTRACT

The flow transient critical heat fluxes (FT-CHFs, $q_{cr,sub}$) in a SUS304-circular tube caused by a rapid decrease in velocity from non-boiling regime are systematically measured for various initial flow velocities, initial heat fluxes, inlet liquid temperatures, outlet pressures and decelerations caused by a rapid decrease in velocity by the experimental water loop comprised of a multistage canned-type circulation pump controlled by an inverter. The SUS304-circular tubes of inner diameter (d=6 mm), heated length (L=59.5 mm), L/d (=9.92) and wall thickness (δ=0.5 mm) with average surface roughness (Ra=3.89 μm) are used in this work. The flow transient CHFs for SUS304-circular tube are compared with authors' steady-state CHF data for the empty VERTICAL and HORIZONTAL SUS304-circular tubes and the values calculated by authors' steady-state CHF correlations against outlet and inlet subcoolings for the empty circular tube. The influences of initial flow velocity (u_0), initial heat flux (q_0) and deceleration caused by a rapid decrease in velocity (α) on the flow transient CHF are investigated into details and the widely and precisely predictable correlations of CHF and flow velocity at the flow transient CHF for the circular tube is given based on the experimental data. The correlations can describe the flow velocity and the CHFs at the flow transient CHFs for SUS304-circular tube obtained in this work within ±20 % difference.

Key Words:

Transient Critical Heat Flux, Subcooled Water Flow Boiling, SUS304-Circular Tube, Rapid Decrease in Velocity, Deceleration, Non-Boiling Regime

INTRODUCTION

Flow transient critical heat fluxes of subcooled water flow boiling in a SUS304-circular tube caused by a rapid decrease in velocity from non-boiling regime is necessary to investigate the reliability of a divertor in a nuclear fusion facility at a loss of flow accident. The nuclear fusion facility has two operation modes. One is the steady-state operation mode, and the other is the transient one. The plasma facing material in transient operation mode is exposed to a heat load three times larger or more than during steady-state operation for several seconds. The knowledge of high heat flux heat removal during various decelerations caused by the rapid decreases in velocity (flow transients) becomes especially very important to take the heat out of the plasma facing material for short pulse high heat flux test mode. The influence of deceleration caused by a rapid decrease in velocity on transient CHF in subcooled water flow will be immediately supposed to be applied to thermal analysis of the divertor of a helical type fusion experimental device which is Large Helical Device (LHD) located in National Institute for Fusion Science (NIFS), Japan.

Many researchers have experimentally studied the steady state CHFs uniformly heated on the circular tube with and without twisted-tape insert by a steadily increasing current at a fixed mass velocity for Fusion Reactor Safety (FRS), shown that the circular tube with twisted-tape insert provide considerable enhancement of CHFs in subcooled flow boiling and given the correlations for calculating CHFs on the circular tube with twisted-tape insert [1-9]. We have supposed that the enhancement of CHFs for the circular tube with twisted-tape insert will be due to reduction of conductive sub-layer thickness on heated surface of test tube and due to an increase in liquid flow velocity from straight flow to swirl one, not new mechanism of heat transfer crisis. And furthermore, we have also supposed that flow velocity will affect the incipient boiling superheat and the nucleate boiling heat transfer up to the CHF. Incipient boiling superheat may shift to a very high value at higher flow velocity and a direct transition to film boiling or a trend of a decrease in CHF with a delay of boiling initiation may occur due to the heterogeneous spontaneous nucleation but not due to the hydro-dynamic instability. The accurate measurement for the subcooled boiling heat transfer up to the CHF is necessary to clarify a change in the mechanism of CHF.

Recently, we systematically measured the power transient critical heat fluxes (PT-CHFs) of subcooled water flow boiling in a SUS304-circular tube for the inner diameter (d=6 mm), the heated length (L=59.4 mm), the effective length (L_{eff}=49.4 mm), L/d (=9.9), L_{eff}/d (=8.23) and the wall thickness (δ=0.5 mm) with the twisted-tape of width (w=5.6 mm), thickness (δ_T=0.6 mm), total length (l=372 mm) and twist ratios, y [H/d=(pitch of 180° rotation)/d], of 2.40, 3.37 and 4.45 for the mass velocities (G=3988 to 13620

kg/m^{2}s), the inlet liquid temperatures (T_{in}=287.55 to 313.14 K), the outlet pressures (P_{out}=805.11 to 870.23 kPa) and the exponentially increasing heat inputs ($Q=Q_0 exp(t/\tau)$, τ=26.85 ms to 8.43 s). The influences of twisted-tape insert, twist ratio, heating rate and swirl velocity on the transient CHF are investigated into details. And the power transient CHF correlations against inlet and outlet subcoolings for the test tubes with twisted-tape insert are derived due to the effect of boiling number based on swirl velocity, $Bo_{cr,sw}$, and Weber number based on swirl velocity, We_{sw} [10-13].

$$Bo_{cr,sw} = C_1 D^{*-0.1} We_{sw}^{-0.3} \left(\frac{L}{d}\right)^{-0.1} e^{-\frac{(L/d)}{C_2 Re_d^{0.4}}} Sc^{*C_3} \times \left(1 + 11.4 p^{*-0.6}\right) \quad \text{if inlet subcooling is known } (\Delta T_{sub,in} \geq 40 \text{ K}) \tag{1}$$

$$Bo_{cr,sw} = 0.082 D^{*-0.1} We_{sw}^{-0.3} \left(\frac{L}{d}\right)^{-0.1} Sc^{0.7} \times \left(1 + 6.34 p^{*-0.6}\right) \quad \text{if outlet subcooling is known } (\Delta T_{sub,out} \geq 30 \text{ K}) \tag{2}$$

where $$Bo_{cr,sw} = \frac{q_{cr,sub,st}}{Gh_{fg}} \times \frac{(\pi d^2 - 4w\delta_T)}{\pi d^2} \times \frac{2y}{(4y^2 + 2\pi^2)^{0.5}} \tag{3}$$

$$We_{sw} = \frac{G^2 d}{\rho_l \sigma} \times \left(\frac{\pi d^2}{\pi d^2 - 4w\delta_T}\right)^2 \times \left[\frac{(4y^2 + 2\pi^2)^{0.5}}{2y}\right]^2 \tag{4}$$

C_1=0.082, C_2=0.53 and C_3=0.7 for L/d≤around 40 and C_1=0.092, C_2=0.85 and C_3=0.9 for L/d>around 40. p^*, w, δ_T and y are the non-dimensional exponential period [$\tau u/\{\sigma/g/(\rho_l-\rho_g)\}^{0.5}$], the width of the twisted-tape, the thickness of the twisted-tape and the twist ratio of the twisted-tape [H/d=(pitch of 180° rotation)/d], respectively. Most of the power transient CHF data for SUS304-circular tubes of d=6 mm with the twisted-tapes of twist ratios, y, of 2.40, 3.37 and 4.45 (186 points) are within -26.19 to 9.81 % difference of Eq. (1) and within -25.22 to 14.03 % one of Eq. (2) for the wide ranges of non-dimensional exponential periods (p^*=48.21 to 5.052×10^4) and swirl velocities (u_{sw}=5.04 to 20.72 m/s).

The objectives of present study at a loss of flow accident for Fusion Reactor Safety (FRS) are fivefold. First is to measure the transient critical heat fluxes for SUS304-circular tube with various decelerations caused by a rapid decrease in velocity (α) for the wide ranges of initial flow velocities (u_0), initial heat fluxes (q_0) and inlet subcoolings ($\Delta T_{sub,in}$). Second is to compare the above results with the power transient critical heat fluxes for SUS304-circular tubes with and without twisted-tape inserts caused by rapid increasing heat inputs [10-18] (PT-CHF). Third is to clarify the influence of initial flow velocity, initial heat flux, inlet subcooling and deceleration caused by a rapid decrease in velocity on the flow transient critical heat flux (FT-CHF). Fourth is to derive the correlations of flow velocity and CHF at the flow transient critical heat flux in a circular tube based on the experimental data. Fifth is to discuss the mechanism of the subcooled flow boiling critical heat flux in a circular tube.

EXPERIMENTAL APPARATUS AND METHOD

Experimental Water Loop

The schematic diagram of experimental water loop is shown in Fig. 1. The loop is made of SUS304 stainless steel and is capable of working up to 2 MPa. The loop has five test sections whose inner diameters are 2, 3, 6, 9 and 12 mm. Test sections were vertically oriented with water flowing upward. The test section of the inner diameter of 6 mm was used in this work. The circulating water was distilled and deionized with about 0.2-μS/cm specific resistivity. The circulating water through the loop was heated or cooled to keep a desired inlet temperature by pre-heater or cooler. The mass velocity was measured by a mass flow meter using a vibration tube (Nitto Seiko, CLEANFLOW 63FS25, Flow range=100 and 750 kg/min). The mass velocity was controlled by regulating the frequency of the three-phase alternating power source to the multistage canned-type circulation pump with high pump head (Nikkiso Co., Ltd., Non-Seal Pump Multi-stage Type VNH12-C4 C-3S7SP, pump flow rate=12 m^3/h, pump head=250 m) with an inverter installed a 4-digit LED monitor (Mitsubishi Electric Corp., Inverter, Model-F720-30K). The pump input frequency shows the net pump input power and pump discharge pressure free of slip loss. The circulating water was pressurized by saturated vapor in the pressurizer in this work. The pressure at the outlet of the test tube was controlled within ±1 kPa of a desired value by using a heater controller of the pressurizer.

Test Section

The cross-sectional view of 6 mm inner diameter test section used in this work is shown in Fig. 2. The SUS304 test tubes with 3 different surface roughnesses have been generally used. The test tubes with rough and smooth finished inner surfaces (RF and SF) are commercially available. The rough finished inner surface was fabricated by annealing the test tube first in the atmosphere of air and was then acidized. The rough finished inner surface test tube (RF) was used in this work. The SUS304 circular tubes for the test tube inner diameter of 6 mm and the heated lengths, L, of 59.5 to 59.7 mm were mainly used. Wall thickness of the test tube, δ, was 0.5 mm. Two fine 0.07-mm diameter platinum wires were spot-welded on the outer surface of the test tube as potential taps. The effective lengths, L_{eff}, of the test tube between the potential taps on which heat transfer was measured were 48.7 to 50.2 mm. The silver-coated 5-mm thickness copper-electrode-plates to supply heating current were soldered to the surfaces of the both ends of the test tube. The both ends of test tube were electrically isolated from the loop by Bakelite plates of 14-mm thickness. The outer surface condition of the test tube was exposed to the atmosphere due to supporting two fine potential taps in this work. The inner surface condition of the test tube was observed by the scanning electron microscope (SEM) photograph (JEOL JXA8600) and inner surface roughness was measured by Tokyo Seimitsu Co., Ltd.'s surface texture measuring instrument (SURFCOM 120A). Figure 3 shows the SEM photograph for the

SUS304 test tube of d=6 mm with the rough finished inner surface (RF). The inner surface roughness is measured 3.89 μm for *Ra*, 21.42 μm for *Rmax* and 15.03 μm for *Rz*.

Method of Heating Test Tube

The test tube has been heated with a fixed heat input supplied from a direct current source (Takasago Ltd., NL035-500R, DC 35 V-3000 A) through the two copper electrodes shown in Fig. 4. The common specifications of the direct current source are as follows. Constant-voltage (CV) mode regulation is 0.005 %+3 mV of full scale, CV mode ripple is 500 μV r.m.s. or better and CV mode transient response time is less than 200 μsec (Typical) against 5 % to full range change of load. The flow transient CHFs, $q_{cr,sub}$, were realized by a rapid decrease in flow velocity from non-boiling regime on the test tube. At the flow transient CHF, the test tube average temperature rapidly increases. The current for the heat input to the test tube was automatically cut off when the measured average temperature increased up to the preset temperature, which was several tens of Kelvin higher than corresponding flow transient CHF surface temperature. This procedure avoided actual burnout of the test tube.

Measurement of Flow Transient CHF, Temperature and Pressure for Test Tube

The flow transient average temperature of the test tube, $\bar{T}(t)$, was measured with resistance thermometry participating as a branch of a double bridge circuit for the temperature measurement. The output voltages from the bridge circuit, $V_T(t)$, together with the voltage drop across the potential taps of the test tube, $V_R(t)=I(t)R_T(t)$, and across a standard resistance, $V_I(t)=I(t)R_s$, were amplified and then were sent via a D/A converter to a digital computer. The unbalance voltage, $V_T(t)$, is expressed by means of Ohm's low as the following form.

$$V_T(t) = \frac{I(t)\{ R_T(t) \times R_2 - R_1 \times R_3 \}}{R_2 + R_3} \tag{5}$$

These voltages were simultaneously sampled at a constant interval ranging from 120 μs to 200 ms. The average temperature of the test tube between the potential taps was calculated with the aid of previously calibrated resistance-temperature relation, $R_T(t)=a(1+b\bar{T}(t)+c\bar{T}(t)^2)$. The average temperatures of the test tube between the two electrodes, $V_{R1}(t)$, were compared with those between potential taps, $V_R(t)$, and much difference for a heat loss could not be clearly observed in high subcooling range.

The heat generation rate, $Q(t)=I^2(t)R_T(t)$, in the test tube between the potential taps was calculated from the measured voltage difference between the potential taps of the test tube and the standard resistance, $V_R(t)$ and $V_I(t)$. The surface heat flux, $q(t)$, is the difference between the heat generation rate per unit surface area, $Q(t)$, and the rate of change of energy storage in the test tube obtained

from the faired average temperature versus time curve as follows:

$$q(t)=\frac{V}{S}\left(Q(t)-\rho c\frac{d\bar{T}(t)}{dt}\right) \tag{6}$$

where ρ, c, V and S are the density, the specific heat, the volume and the inner surface area of the test tube, respectively.

The heater inner surface temperatures between the two potential taps, $T_s(t)$, were also obtained by solving the unsteady heat conduction equation in the test tube under the conditions of measured average temperature, $\bar{T}(t)$, and heat generation rate per unit surface area, $Q(t)$, of the test tube. All the calculations of the inner surface temperature were made by using the PHOENICS code [19]. Basic unsteady two-dimensional heat conduction equation for the test tube is as follows:

$$\rho c\frac{\partial T}{\partial t}=\frac{1}{r}\frac{\partial}{\partial r}\left(\lambda r\frac{\partial T}{\partial r}\right)+\frac{1}{r}\frac{\partial}{\partial \theta}\left(\frac{\lambda}{r}\frac{\partial T}{\partial \theta}\right)+Q(t) \tag{7}$$

The calculation domain from test tube inner radius, r_i, to test tube outer radius, r_o, is radially divided into 500 grid points (Δr=1 μm) and the time step, Δt, is given much smaller than 0.45 ms. The unsteady equation is numerically analyzed together with the following boundary conditions.

$$q(t)=-\lambda\left.\frac{\partial T}{\partial r}\right|_{r=r_i} \tag{8}$$

$$\left.\frac{\partial T}{\partial r}\right|_{r=r_o}=0 \tag{9}$$

Furthermore, the steady-state inner and outer surface temperatures, T_s and T_{so}, were also obtained by solving the heat conduction equation in the test tube under the conditions of measured average temperature, $\bar{T}$, and surface heat flux, q, of the test tube. The solutions for the inner and outer surface temperatures of the test tube, T_s and T_{so}, are given by the steady one-dimensional heat conduction equation. The basic equation for the test tube is as follows:

$$\frac{d^2T}{dr^2}+\frac{1}{r}\frac{dT}{dr}+\frac{Q}{\lambda}=0 \tag{10}$$

then integration yields and the mean temperature of the test tube is obtained.

$$T(r)=-\frac{Qr^2}{4\lambda}+\frac{Qr_o^2}{2\lambda}\ln r+C \tag{11}$$

$$\bar{T}=\frac{1}{\pi\left(r_o^2-r_i^2\right)}\int_{r_i}^{r_o}2\pi rT(r)dr \tag{12}$$

Generating heat in the tube is equal to the heat conduction and the test tube is perfectly insulated.

$$q = -\lambda \left.\frac{dT}{dr}\right|_{r=r_i} = \frac{\left(r_o^2 - r_i^2\right)Q}{2r_i} \tag{13}$$

$$\left.\frac{dT}{dr}\right|_{r=r_o} = 0 \tag{14}$$

The temperatures of the heater inner and outer surfaces, T_s and T_{so}, and C in Eq. (11) can be described by the steady one-dimensional heat conduction equation as follows:

$$T_s = T(r_i) = \overline{T} - \frac{qr_i}{4(r_o^2 - r_i^2)^2\lambda} \times \left[4r_o^2 \left\{ r_o^2 \left(ln r_o - \frac{1}{2} \right) - r_i^2 \left(ln r_i - \frac{1}{2} \right) \right\} - \left(r_o^4 - r_i^4 \right) \right] - \frac{qr_i}{2(r_o^2 - r_i^2)\lambda} \left(r_i^2 - 2r_o^2 \, ln r_i \right) \tag{15}$$

$$T_{so} = T(r_o) = \overline{T} - \frac{qr_i}{4(r_o^2 - r_i^2)^2\lambda} \times \left[4r_o^2 \left\{ r_o^2 \left(ln r_o - \frac{1}{2} \right) - r_i^2 \left(ln r_i - \frac{1}{2} \right) \right\} - \left(r_o^4 - r_i^4 \right) \right] - \frac{qr_i r_o^2}{2(r_o^2 - r_i^2)\lambda} \left(1 - 2 ln r_o \right) \tag{16}$$

$$C = \overline{T} - \frac{qr_i}{4(r_o^2 - r_i^2)^2\lambda} \times \left[4r_o^2 \left\{ r_o^2 \left(ln r_o - \frac{1}{2} \right) - r_i^2 \left(ln r_i - \frac{1}{2} \right) \right\} - \left(r_o^4 - r_i^4 \right) \right] \tag{17}$$

where $\overline{T}$, q, λ, r_i and r_o are average temperature of the test tube, heat flux, thermal conductivity, test tube inner radius and test tube outer radius, respectively.

In case of the 6 mm inner diameter test section, before entering the test tube, the test water flows through the tube with the same inner diameter of the test tube to form the fully developed velocity profile. The entrance tube length, l_e, is given 333 mm (l_e/d=55.5). The values of l_e/d for d=6 mm in which the center line velocity reaches 99 % of the maximum value for turbulence flow were obtained ranging from 9.8 to 21.9 by the correlation of Brodkey and Hershey [20] as follows:

$$\frac{l_e}{d} = 0.693 \, Re_d^{1/4} \tag{18}$$

The inlet and outlet liquid temperatures were measured by 1-mm o.d., sheathed, K-type thermocouples (*Nimblox*, sheath material: SUS316, hot junction: ground, response time (63.2 %): 46.5 ms) which are located at the centerline of the tube at the upper and lower stream points of 283 and 63 mm from the test tube inlet and outlet points. The inlet and outlet pressures were measured by the strain gauge transducers (Kyowa Electronic Instruments Co., Ltd., PHS-20A, Natural frequency: approximately 30 kHz), which were located near the entrance of conduit at upper and lower stream points of 63 mm from the test tube inlet and outlet points. The thermocouples and the transducers were installed in the conduits as shown in Fig. 2. The inlet and outlet pressures were calculated from the pressures measured by inlet and outlet pressure transducers as follows:

$$P_{in} = P_{ipt} - \left\{ \left(P_{ipt} \right)_{wnh} - \left(P_{opt} \right)_{wnh} \right\} \times \frac{L_{ipt}}{L_{ipt} + L + L_{opt}} \tag{19}$$

$$P_{out} = P_{in} - \left(P_{in} - P_{opt} \right) \times \frac{L}{L + L_{opt}} \tag{20}$$

where L_{ipt}=0.063 m and L_{opt}=0.063 m.

Experimental errors are estimated to be ±1 K in inner tube surface temperature and ±2 % in heat flux. Mass velocity, inlet and outlet subcoolings, inlet and outlet pressures and deceleration caused by a rapid decrease in velocity were measured within the accuracy ±2 %, ±1 K, ±4 kPa and ±2 %, respectively.

Flow transient CHF experiments at a loss of flow were performed as follows. Liquid level in the pressurizer was adjusted to about 400 mm from the bottom of the vessel. Pressure of the test loop was kept constant at around 800 kPa by saturated vapor heated in the pressurizer. The circulation pump controlled by an inverter was turn on and the pump input frequency (f_{pi}) kept constant at a flow velocity, u, of 4.0 m/s. Inlet liquid temperature in the test loop was raised and kept constant at the desired value of ranging from 290 to 308 K by using the pre-heater or cooler. First of all steady-state critical heat fluxes in a circular test tube caused by exponentially increasing heat input ($Q_0 \exp(t/\tau)$, τ=around 8 s) were measured. Then, the initial pump input frequency (f_{pi0}) was raised and kept constant at a initial flow velocities (u_0=6.9, 9.9 or 13.3 m/s) and electric current to the test tube was gradually raised to a desired heat generation rate level which is the value of CHF measured by exponentially increasing heat input at the flow velocity of 4 m/s. Then the pump input frequency was linearly reduced to 0 Hz for a deceleration time setting, t_d, ranging from 0 to 200 seconds by the inverter function (rapidly to gradually). Schematic diagram of time variations in pump input frequency and flow velocity for flow transient CHF experiment are shown in Fig. 5. The heat generation rate, $Q(t)=I^2(t)R_T(t)$, in the test tube was kept constant for 144 ms to 240 s during which the measurements were made in the time intervals of 120 μs to 200 ms (1200 points) at each deceleration caused by a rapid decrease in velocity.

EXPERIMENTAL RESULTS AND DISCUSSION

Experimental Conditions

Flow transient heat transfer processes and CHFs that caused by a rapid decrease in velocity, $u(t)=u_0-\alpha t$, were measured for the SUS304-circular tube. The deceleration caused by a rapid decrease in velocity (α) ranged from -7.357 to -0.326 m/s^2. The initial experimental conditions such as mass velocity, inlet subcooling, outlet pressure and initial heat flux in flow transient heat transfer and CHF experiments with various decelerations caused by a rapid decrease in velocity were determined independently each other before

each experimental run.

The experimental conditions were as follows:

Test Tube Number	THD-F191 to THD-F196
Test Tube Material	SUS304
Inner Diameter (d)	6 mm
Heated Length (L)	59.5 to 59.7 mm
Effective Length (L_{eff})	48.7 to 50.2 mm
L/d	9.92 to 9.95
L_{eff}/d	8.12 to 8.37
Wall Thickness (δ)	0.5 mm
Surface Condition	Rough finished inner surface (commercial finish)
Surface Roughness	3.89 μm for *Ra*, 21.42 μm for *Rmax* and 15.03 μm for *Rz*
Mass Velocity (G)	0 to 13610 kg/m^{2}s
Initial Flow Velocity (u_0)	7.057 to 13.635 m/s for conditions of u_0=6.9, 9.9 and 13.3 m/s
Inlet Pressure (P_{in})	717.56 to 1448.74 kPa
Outlet Pressure (P_{out})	698.38 to 1288.97 kPa
Inlet Subcooling ($\Delta T_{sub,in}$)	134.00 to 164.88 K
Outlet Subcooling ($\Delta T_{sub,out}$)	77.67 to 116.39 K
Inlet Liquid Temperature (T_{in})	290.12 to 308.51 K
Initial heat flux (q_0)	15.59 to 17.34 MW/m^2
Deceleration caused by a Rapid Decrease in Velocity (α)	-7.357 to -0.326 m/s^2

Steady-state Subcooled Flow Boiling CHF Characteristics [21-23]

Outlet subcooling: Figure 6 shows the steady-state CHFs, $q_{cr,sub,st}$, versus the outlet subcoolings, $\Delta T_{sub,out}$, for the HORIZONTAL SUS304 circular test tube of the inner diameter (d=6 mm), the heated length (L=59.4 mm), L/d (=9.9) and the wall thickness (δ=0.5 mm) obtained for the flow velocities, u, ranging from 4 to 13.3 m/s at the outlet pressure, P_{out}, of around 800 kPa. The CHF data for the VERTICAL SUS304 test tube of d=6 mm, L=66 mm, L/d=11 and δ=0.5 mm with the flow velocities ranging from 4.0 to 13.3 m/s are also shown in the figure for comparison [22]. As shown in the figure, the $q_{cr,sub,st}$ for each flow velocity become

higher with an increase in $\Delta T_{sub,out}$ and the increasing rate becomes lower for higher $\Delta T_{sub,out}$. The CHFs in the whole experimental range become higher with an increase in the flow velocity at a fixed $\Delta T_{sub,out}$. The curves given by the steady-state CHF correlation against outlet subcooling, Eq. (21), for the VERTICAL SUS304 circular test tube are shown in Fig. 6 at each flow velocity for comparison. The exponential periods, τ, of the heat input, $Q=Q_0 \exp(t/\tau)$, ranged from 6.55 to 21.81 s.

$$Bo_{cr} = 0.082 D^{*-0.1} We^{-0.3} \left(\frac{L}{d}\right)^{-0.1} Sc^{0.7} \qquad \text{for } \Delta T_{sub,out} \geq 30 \text{ K and } u \leq 13.3 \text{ m/s} \tag{21}$$

C_1=0.082, C_2=0.53 and C_3=0.7 for $L/d \leq$around 40 and C_1=0.092, C_2=0.85 and C_3=0.9 for $L/d >$around 40. The CHF data for $\Delta T_{sub,out} \geq 30$ K are in good agreement with the values given by the correlation. Equation (21) was derived based on the experimental data for the VERTICAL SUS304 test tube with the flow velocity ranging from 4 to 13.3 m/s. To confirm the applicability of Eq. (21) to the data for the flow velocity of 4 to 13.3 m/s, the ratios of these CHF data to the corresponding values calculated by Eq. (21) are shown versus $\Delta T_{sub,out}$ in Fig. 7. Most of the data for the HORIZONTAL circular test tube (69 points) and the VERTICAL one (110 points) are within ±15 % difference for 4 m/s$\leq u \leq$13.3 m/s and 29.7 K$\leq \Delta T_{sub,out} \leq$125.38 K.

Inlet subcooling: It can be considered that the CHFs are determined not by the outlet conditions but by the inlet ones. The steady-state CHFs, $q_{cr,sub,st}$, for the HORIZONTAL SUS304 circular test tube of the inner diameter of 6 mm, L=59.4 mm, L/d=9.9 and δ=0.5 mm were shown versus the inlet subcooling, $\Delta T_{sub,in}$, with the flow velocities of 4 to 13.3 m/s in Fig. 8. The CHF data for the VERTICAL SUS304 test tube of d=6 mm, L=66 mm, L/d=11 and δ=0.5 mm with the flow velocities ranging from 4.0 to 13.3 m/s are also shown in the figure for comparison [23]. The $q_{cr,sub,st}$ for each flow velocity become higher with an increase in $\Delta T_{sub,in}$. The increasing rate becomes also lower for higher $\Delta T_{sub,in}$. The $q_{cr,sub,st}$ increase with an increase in the flow velocity at a fixed $\Delta T_{sub,in}$. The $q_{cr,sub,st}$ for the wide range of flow velocities are proportional to $\Delta T_{sub,in}^{0.7}$ for $\Delta T_{sub,in} \geq 40$ K. The curves derived from the steady-state CHF correlations against inlet subcooling, Eq. (22), for the VERTICAL SUS304 circular test tube are shown in Fig. 8 for comparison.

$$Bo_{cr} = C_1 D^{*-0.1} We^{-0.3} \left(\frac{L}{d}\right)^{-0.1} e^{-\frac{(L/d)}{C_2 Re_d^{0.4}}} Sc^{*C_3} \qquad \text{for } \Delta T_{sub,in} \geq 40 \text{ K and } u \leq 13.3 \text{ m/s} \tag{22}$$

The CHF data for $\Delta T_{sub,in} \geq 40$ K are in good agreement with the values given by authors' correlation. To confirm the applicability of Eq. (22), the ratios of these CHF data for the d=6 mm HORIZONTAL circular test tube (69 points) and those for the d=6 mm VERTICAL one (110 points) to the corresponding values calculated by Eq. (22) are shown versus $\Delta T_{sub,in}$ in Fig. 9. Most of the data for $\Delta T_{sub,in} \geq 40$ K are within ±15 % difference of Eq. (22) for the wide ranges of inlet subcoolings and flow velocities.

Flow Transient CHF Characteristics (Current Study)

In case of initial flow velocity, u_0, of 6.9 m/s at initial heat Flux, $q_0=(q_{cr,sub,st})_{u=4m/s}$: Figure 10 shows typical example of the time variations in the inlet and outlet pressures, P_{in} and P_{out}, the inlet and outlet liquid temperatures, T_{in} and T_{out}, heater inner surface temperature, T_s, heat flux, q, and inlet flow velocity, u, for the initial flow velocity, u_0=7.09 m/s, the initial heat flux, q_0=15.73 MW/m^2, which is equivalent to the CHF measured by exponentially increasing heat input ($Q_0 \exp(t/\tau)$, τ=around 8 s) at the flow velocity of 4 m/s and deceleration caused by a rapid decrease in velocity, α=-1.771 m/s^2, at initial outlet pressure, P_{out0}=801.37 kPa, initial inlet subcooling, $\Delta T_{sub,in0}$=145.83 K. The values of P_{in}, P_{out}, T_{in}, T_{out}, T_s, q and u keep almost constant until the beginning of a decrease in flow velocity. The pump input frequency was linearly reduced to 0 Hz at a deceleration time setting, t_d, of 20 seconds by the inverter function. As soon as the inlet flow velocity decreases, the P_{in} and P_{out} oscillate violently and the T_s and T_{out} have started to increase. At the elapsed time of 6.35 seconds, that is, the flow transient CHF point, the heater inner surface temperature, T_s, rapidly increases, although the heat flux, $q_{cr,sub}$, oppositely decreases at the flow transient CHF. The current for the heat input to the test tube was automatically cut off when the measured average temperature increased up to the preset temperature, which was several tens of Kelvin higher than corresponding flow transient CHF surface temperature. This procedure avoided actual burnout of the test tube. The heat flux, the outlet pressure, P_{out}, the flow velocity, u_{cr}, and the deceleration caused by a rapid decrease in velocity, α, at the flow transient CHF were measured 17.726 MW/m^2, 703.29 kPa, 4.56 m/s and -1.771 m/s^2 in this run.

Figure 11 shows the time variations in P_{in}, P_{out}, T_{in}, T_{out}, T_s, q and u for the u_0=7.10 m/s, q_0=15.81 MW/m^2 and α=-3.756 m/s^2, at P_{out0}=805.19 kPa, $\Delta T_{sub,in0}$=145.69 K. The values of P_{in}, P_{out}, T_{in}, T_{out}, T_s, q and u keep also constant until the beginning of a decrease in flow velocity. The pump input frequency was linearly reduced to 0 Hz at a deceleration time setting of 0 second by the inverter function. The heat flux, the outlet pressure, the flow velocity and the deceleration caused by a rapid decrease in velocity at the flow transient CHF were measured 18.244 MW/m^2, 812.75 kPa, 6.69 m/s and -3.756 m/s^2 in this run. The flow velocity at the flow transient CHF point becomes 46.7 % higher (from 4.56 to 6.69 m/s) with a decrease in the deceleration caused by a rapid decrease in velocity, α, from -1.771 to -3.756 m/s^2 at the initial flow velocity, u_0=7.09 m/s.

In case of initial flow velocity, u_0, of 9.9 m/s at initial heat Flux, $q_0=(q_{cr,sub,st})_{u=4m/s}$: Figures 12 and 13 show typical examples of the time variations in P_{in}, P_{out}, T_{in}, T_{out}, T_s, q and u for u_0=10.09 and 10.08 m/s, q_0=16.78 and 16.70 MW/m^2 and α=-3.260 and -5.444 m/s^2 with the deceleration time setting 10 and 0 seconds at P_{out0}=829.89 and 830.62 kPa, and $\Delta T_{sub,in0}$=150.56 and 149.85 K, respectively. The values of P_{in}, P_{out}, T_{in}, T_{out}, T_s, q and u keep also constant until the beginning of a decrease in flow velocity. The heat fluxes, the outlet pressures, the flow velocities and the decelerations caused by a rapid decrease in velocity at the flow transient CHF

were measured 19.46 and 19.373 MW/m^2, 990.96 and 732.48 kPa, 6.09 and 8.61 m/s, and -3.26 and -5.444 m/s^2 in these runs, respectively. The flow velocity at the flow transient CHF point becomes 41.4 % higher (from 6.09 to 8.61 m/s) with a decrease in the deceleration caused by a rapid decrease in velocity from -3.26 to -5.444 m/s^2 at the initial flow velocity, u_0=10.09 m/s.

In case of initial flow velocity, u_0, of 13.3 m/s at initial heat Flux, $q_0=(q_{cr,sub,st})_{u=4m/s}$: Figures 14 and 15 show typical examples of the time variations in P_{in}, P_{out}, T_{in}, T_{out}, T_s, q and u for u_0=13.30 and 13.26 m/s, q_0=16.62 and 16.51 MW/m^2 and α=-5.076 and -7.357 m/s^2 for the deceleration time setting 7 and 2 seconds at P_{out0}=842.63 and 843.60 kPa, and $\Delta T_{sub,in0}$=155.21 and 156.32 K, respectively. The values of P_{in}, P_{out}, T_{in}, T_{out}, T_s, q and u keep also constant until the beginning of a decrease in flow velocity. The heat fluxes, the outlet pressures, the flow velocities and the decelerations caused by a rapid decrease in velocity at the flow transient CHF were measured 18.979 and 17.994 MW/m^2, 791.29 and 771.49 kPa, 7.20 and 10.41 m/s, and -5.076 and -7.357 m/s^2 in these runs, respectively. The flow velocity at the flow transient CHF point becomes 44.6 % higher (from 7.20 to 10.41 m/s) with a decrease in the deceleration caused by a rapid decrease in velocity from -5.076 to -7.357 m/s^2 at the initial flow velocity, u_0=13.30 m/s.

For **power transient CHF experiments**, the rate of increasing heat input is very high. It takes time to form the fully developed temperature profile in the test tube because the test tube has some heat capacity. Then the temperature profile in the conductive sub-layer on the test tube surface grows, and vaporization occurs. It also takes some time to occur instantaneously the heterogeneous spontaneous nucleation on the test tube surface at the power transient CHF. Namely, it is explained to be as a result of the time-lag of the formation of the power transient CHF for the increasing rate of the heat input. However, for **flow transient CHF experiments**, the deviations from the radial flow velocity for isothermal flow are a result of the fact that the decrease in flow velocity advances at the vicinity of the tube surface on the test section and is late at the center of the tube on the test section by interaction of a tube wall surface and the test water in the viscosity. Namely, it is explained to be as a result of the non-uniform of the decreasing rate of the radial flow velocity for the formation of the flow transient CHF.

The flow transient CHFs, $q_{cr,sub}$, at the initial heat flux, $q_0=(q_{cr,sub,st})_{u=4m/s}$, which is equivalent to the CHF measured by exponentially increasing heat input ($Q_0 \exp(t/\tau)$, τ=around 8 s) at the flow velocity of 4 m/s, for the decelerations caused by a rapid decrease in velocity, α, ranging from -7.357 m/s^2 to -0.326 m/s^2 are shown as green, orange and sky-blue open circle symbols with the initial flow velocities, u_0, of 6.9, 9.9 and 13.3 m/s, respectively, in Figs. 6 to 9. Most of the flow transient CHF data are within -34.1 to 15.4 % and -39.7 to 0.55 % differences of the values calculated from the steady-state CHF correlations against outlet and inlet subcoolings for the circular test tube, Eqs. (21) and (22), respectively.

Figure 16 shows a typical photograph for SUS304 test tubes of d=6 mm and L=59.7 mm with the test tube numbers of THD-F192

and THD-F194 burned out in flow transient CHF experiments. The dark sections in the middle to outlet of the test tube are the traces of the vapor patches which would have become high temperature; the local temperatures on the tube jumped to those of the film boiling region at the occurrence of flow transient CHF. The locations of these vapor patches were almost observed in the middle to outlet of the test tube in this flow transient CHF experiment. It is assumed that the transition to film boiling in this work would occur by two mechanisms of the subcooled flow boiling critical heat flux: one is due to the hydro-dynamic instability at an outlet area of the test tube and the other is due to the heterogeneous spontaneous nucleation at the lower limit of the heterogeneous spontaneous nucleation temperature at a middle area of the test tube. The tube wall did not clearly melt down along the circumference of the tube, because the heating current to the tube was instantaneously cut off when the measured average temperature rapidly increased up to the preset temperature lower than the actual burnout temperature of the tube. By using this burnout detector, several CHF data were obtained for a single tube without the actual burnout.

Correlations of Flow Velocity and CHF at Flow Transient CHF

The experimental results of the flow transient CHFs for d=6 mm inner diameter at the initial heat flux, $q_0=(q_{cr,sub,st})_{u=4m/s}$, which is equivalent to the CHF measured by exponentially increasing heat input ($Q_0 \exp(t/\tau)$, τ=around 8 s) at the flow velocity of 4 m/s with the initial flow velocities, u_0, of 6.9, 9.9 and 13.3 m/s are shown in Fig. 17 on the flow velocity at flow transient CHF, u_{cr}, versus the deceleration caused by a rapid decrease in velocity, α, graph and on the flow transient CHF, $q_{cr,sub}$, versus α graph with the initial flow velocity as a parameter. The u_{cr} become linearly higher with the decrease in the α from around -1 m/s^2 and are constant for the α greater than -1 m/s^2 and equivalent to 4 m/s. The slopes on the linear graph are almost constant about -1.0 s for the α ranging from -7.357 to -1 m/s^2 and 0 s for the α ranging from -1 to -0.326 m/s^2, respectively. These data for the flow velocity at flow transient CHF, u_{cr}, can be expressed by the following empirical correlations based on the experimental data.

$$u_{cr} = -\alpha + 3 \qquad \text{for } \alpha \leq -1 \text{ m/s}^2 \tag{23}$$

$$u_{cr} = 4 \qquad \text{for } -1 \text{ m/s}^2 < \alpha < -0.326 \text{ m/s}^2 \tag{24}$$

$$q_{cr,sub} = q_0 \qquad \text{for } \alpha < -0.326 \text{ m/s}^2 \tag{25}$$

The correlations can describe the flow transient CHF data (60 points) for d=6 mm with the u_0=6.9, 9.9 and 13.3 m/s at a desired heat flux level which is equivalent to the CHF measured by exponentially increasing heat input ($Q_0 \exp(t/\tau)$, τ=around 8 s) at the flow velocity of 4 m/s, $q_0=(q_{cr,sub,st})_{u=4m/s}$, obtained in this work within ±20 % difference under -7.357 m/s$^2 \leq \alpha \leq$ -0.326 m/s^2 as shown in Fig. 17.

In this study, it is firmly confirmed that the steady-state CHF correlations against outlet and inlet subcoolings, Eqs. (21) and (22), can delineate not only the authors' published CHF data (3206 points) for the HORIZONTAL and VERTICAL SUS304 test tubes with the wide ranges of inlet pressures (P_{in}=159 kPa to 1.1 MPa), inner diameters (d=2 to 12 mm), heated lengths (L=22 to 150 mm) and flow velocities (u=4.0 to 13.3 m/s) [24-32] within ±15 % difference for 30 K≤$\Delta T_{sub,out}$≤140 K and 40 K≤$\Delta T_{sub,in}$≤151 K but also the flow transient CHF for the circular tube of 6 mm inner diameter obtained in this work within -34.1 to 15.4 % and -39.7 to 0.55 % differences, respectively. We have supposed that the expressions of flow velocity map ($u_{cr}/u_{cr,st}$ versus α) and critical heat flux one ($q_{cr,sub}/q_0$ versus α) at flow transient CHF against steady-state critical heat flux would be very useful to discuss the mechanism of the transient critical heat flux of subcooled water flow boiling caused by a rapid decrease in velocity, which would occur due to the hydro-dynamic instability suggested by Kutateladze [33] and Zuber [34] or due to the heterogeneous spontaneous nucleation at the lower limit of the heterogeneous spontaneous nucleation temperature [35]. The ratios of flow velocity at flow transient CHF point to flow velocity calculated from Eq. (22) with initial heat flux, q_0, by a try-and-error method, $u_{cr}/u_{cr,st}$, and those of flow transient CHF, $q_{cr,sub}=q_0$, to steady-state critical heat flux calculated from Eq. (22) with the flow velocity at flow transient CHF point, ($q_{cr,sub}/q_{cr,sub,st}$), for the SUS304 circular test tube of d=6 mm and L=59.5 to 59.7 mm with inlet liquid temperatures, T_{in}, of 290.12 to 308.51 K at the initial flow velocities, u_0, of 6.9, 9.9 and 13.3 m/s are shown versus the deceleration caused by a rapid decrease in velocity, α, at initial heat flux, q_0, which is equivalent to the CHF at the flow velocity of 4 m/s, $(q_{cr,sub,st})_{u=4m/s}$, in Fig. 18. The experimental data of $u_{cr}/u_{cr,st}$ and $q_{cr,sub}/q_{cr,sub,st}$ for the SUS304 test tube of d=6 mm with the rough finished inner surface can be expressed for the α ranging from -7.357 to -0.326 m/s^2 by the following correlations:

$$\frac{u_{cr}}{u_{cr,st}} = -0.275\alpha + 0.794 \qquad \text{for } \alpha \leq -0.75 \text{ m/s}^2 \tag{26}$$

$$\frac{u_{cr}}{u_{cr,st}} = 1 \qquad \text{for } -0.75 \text{ m/s}^2 < \alpha < -0.326 \text{ m/s}^2 \tag{27}$$

$$\frac{q_{cr,sub}}{q_{cr,sub,st}} = 0.05\alpha + 1.038 \qquad \text{for } \alpha < -0.75 \text{ m/s}^2 \tag{28}$$

$$\frac{q_{cr,sub}}{q_{cr,sub,st}} = 1 \qquad \text{for } -0.75 \text{ m/s}^2 < \alpha < -0.326 \text{ m/s}^2 \tag{29}$$

It is assumed that the transition to film boiling at the deceleration caused by a rapid decrease in velocity, α, lower than -5 m/s^2 would occur due to the heterogeneous spontaneous nucleation but not due to the hydro-dynamic instability. The authors' published CHF data (3206 points) for the HORIZONTAL and VERTICAL SUS304 test tubes with the wide ranges of inlet pressures (P_{in}=159 kPa to 1.1

MPa), inner diameters (d=2 to 12 mm), heated lengths (L=22 to 150 mm) and flow velocities (u=4.0 to 13.3 m/s) [24-32] have been measured. In Figs. 19 (a) and (b), the dark sections in the outlet alone of the test tube are the traces of the vapor patches which would have become high temperature; the local temperatures on the tube jumped to those of the film boiling region at the occurrence of steady-state CHF which would occur due to the hydrodynamic instability suggested by Kutateladze [33] and Zuber [34]. The outlet liquid temperature and pressure, T_{out} and P_{out}, become higher and lower respectively and outlet subcooling, $\Delta T_{sub,out}$, does lower, so the transition to film occur at the outlet of the test tube in the first place. In this flow transient CHF experiment, the locations of these vapor patches due to the hydrodynamic instability would be normally observed in the outlet of the test tube at the deceleration caused by a rapid decrease in velocity, α, higher than -5 m/s^2 and those due to the heterogeneous spontaneous nucleation at the lower limit of the heterogeneous spontaneous nucleation temperature would be observed in the middle of the test tube at the α lower than -5 m/s^2. The differences between the locations of the vapor patches in Fig. 16 and those in Figs. 19 (a) and (b) are the reason that the flow transient CHF would occur due to the heterogeneous spontaneous nucleation at the lower limit of the heterogeneous spontaneous nucleation temperature for the rapid flow transient α lower than -5 m/s^2. And, Figure 20 shows the q versus u plots of the transient boiling heat transfer processes on a d=6 mm inner diameter for various decelerations caused by a rapid decrease in velocity, α, of -2.15, -3.63, -5.08, -5.94, -6.60 and -7.36 m/s^2 at a fixed initial flow velocity, u_0, of 13.3 m/s. By comparing the transient heat transfer processes for the α of -2.15, -3.63 and -5.08 m/s^2 with those of -5.94, -6.60 and -7.36 m/s^2, it can be seen that the flow transient critical heat flux for relatively steep deceleration caused by a rapid decrease in velocity is very much affected by the decreasing rate. The transient processes for the α of -2.15, -3.63 and -5.08 m/s^2 successively follow a fixed heat flux with the decrease in the flow velocity and reaches the flow transient critical heat flux, which is expected from the figure to be almost in agreement with the steady-state critical heat flux. On the contrary, those for the α of -5.94, -6.60 and -7.36 m/s^2 follow also a fixed heat flux with the decrease in the flow velocity and reaches the flow transient critical heat flux, which is seen from the figure to be about -30 to 15 % of the steady-state critical heat flux. It is also assumed that the transition to film boiling in this work would occur by two mechanisms of the flow transient critical heat flux: the former is due to the hydro-dynamic instability and the latter is due to the heterogeneous spontaneous nucleation at the lower limit of the heterogeneous spontaneous nucleation temperature.

CONCLUSIONS

The flow transient critical heat fluxes (FT-CHFs) in a SUS304-circular tube for inner diameter (d=6 mm), heated length (L=59.5 to 59.7 mm), effective length (L_{eff}=48.7 to 50.2 mm), L/d (=9.92 to 9.95), L_{eff}/d (=8.12 to 8.37) and wall thickness (δ=0.5 mm) caused by a rapid decrease in velocity from non-boiling regime are systematically measured for initial flow velocities (u_0=7.057 to 13.635 m/s for

conditions of u_0=6.9, 9.9 and 13.3 m/s), initial heat fluxes (q_0=15.59 to 17.34 MW/m^2), inlet liquid temperatures (T_{in}=290.12 to 308.51 K), outlet pressures (P_{out}=698.38 to 1288.97 kPa) and decelerations caused by a rapid decrease in velocity ($u(t)=u_0+\alpha t$, α=-7.357 to -0.326 m/s^2). Experimental results lead to the following conclusions.

1) As soon as the inlet flow velocity decreases, the P_{in} and P_{out} oscillate violently and the T_s and T_{out} have started to increase. At the flow transient CHF point, the heater inner surface temperature, T_s, rapidly increases, although the heat flux, $q_{cr,sub}$, oppositely decreases at the flow transient CHF.
2) Most of the flow transient CHF data are within -34.1 to 15.4 % and -39.7 to 0.55 % differences of the values calculated from the steady-state CHF correlations against outlet and inlet subcoolings for the circular test tube, Eqs. (21) and (22), respectively.
3) The flow velocity at the flow transient CHF point, u_{cr}, becomes linearly higher with a decrease in the deceleration caused by a rapid decrease in velocity, α, from around -1 m/s^2 and are constant for the α greater than -1 m/s^2 and equivalent to 4 m/s.
4) The slopes on the linear graph are almost constant about -1.0 s for the α ranging from -7.357 to -1 m/s^2 and 0 s for the α ranging from -1 to -0.326 m/s^2, respectively. These data for the flow velocity at flow transient CHF, u_{cr}, can be expressed by the following empirical correlations based on the experimental data.

$$u_{cr} = -\alpha + 3 \quad \text{for } \alpha \leq \text{-1 m/s}^2 \tag{23}$$

$$u_{cr} = 4 \quad \text{for -1 m/s}^2 < \alpha < \text{-0.326 m/s}^2 \tag{24}$$

$$q_{cr,sub} = q_0 \quad \text{for } \alpha < \text{-0.326m/s}^2 \tag{25}$$

5) The experimental data of $u_{cr}/u_{cr,st}$ and $q_{cr,sub}/q_{cr,sub,st}$ for the SUS304 test tube of d=6 mm with the rough finished inner surface can be expressed for the α ranging from -7.357 to -0.326 m/s^2 by the following correlations:

$$\frac{u_{cr}}{u_{cr,st}} = -0.275\alpha + 0.794 \quad \text{for } \alpha \leq \text{-0.75 m/s}^2 \tag{26}$$

$$\frac{u_{cr}}{u_{cr,st}} = 1 \quad \text{for -0.75 m/s}^2 < \alpha < \text{-0.326 m/s}^2 \tag{27}$$

$$\frac{q_{cr,sub}}{q_{cr,sub,st}} = 0.05\alpha + 1.038 \quad \text{for } \alpha < \text{-0.75 m/s}^2 \tag{28}$$

$$\frac{q_{cr,sub}}{q_{cr,sub,st}} = 1 \quad \text{for -0.75 m/s}^2 < \alpha < \text{-0.326 m/s}^2 \tag{29}$$

6) We have supposed that the expressions of flow velocity map ($u_{cr}/u_{cr,st}$ versus α) and critical heat flux one ($q_{cr,sub}/q_0$ versus α) at flow transient CHF against steady-state critical heat flux would be very useful to discuss the mechanism of the transient critical heat flux

of subcooled water flow boiling caused by a rapid decrease in velocity, which would occur due to the hydro-dynamic instability or due to the heterogeneous spontaneous nucleation at the lower limit of the heterogeneous spontaneous nucleation temperature. It is assumed that the transition to film boiling at the deceleration caused by a rapid decrease in velocity, α, lower than -5 m/s^2 would occur due to the heterogeneous spontaneous nucleation but not due to the hydro-dynamic instability.

NOMENCLATURE

a, b, c fitted constant

Bo_{cr} $=q_{cr,sub}/Gh_{fg}$, boiling number

$Bo_{cr,sw}$ $= \frac{q_{cr,sub,st}}{Gh_{fg}} \times \frac{(\pi d^2 - 4w\delta_T)}{\pi d^2} \times \frac{2y}{(4y^2 + 2\pi^2)^{0.5}}$, boiling number based on swirl velocity

C constant in Eqs. (11)

C_1, C_2, C_3 constants in Eqs. (1) and (22)

c_p specific heat at constant pressure, J/kg K

D^* $=d/\{\sigma/g/(\rho_l-\rho_g)\}^{0.5}$, non-dimensional diameter

d test tube inner diameter, m

f_{pi} pump input frequency, Hz

f_{pi0} initial pump input frequency, Hz

G $=\rho_l u$, mass velocity, kg/m^{2}s

g acceleration of gravity, m/s^2

h_{fg} latent heat of vaporization, J/kg

I current flowing through standard resistance, A

L heated length, m

L_e entrance length, m

L_{eff} effective length, m

L_{ipt} distance between inlet pressure transducer and inlet of the heated section, m

L_{opt} distance between outlet pressure transducer and outlet of the heated section, m

P pressure, kPa

P_{in} pressure at inlet of heated section, kPa

P_{ipt} pressure measured by inlet pressure transducer, kPa

P_{out} pressure at outlet of heated section, kPa

P_{out0} initial outlet pressure, kPa

P_{opt} pressure measured by outlet pressure transducer, kPa

p^* $= \tau u/\{\sigma/g/(\rho_l-\rho_g)\}^{0.5}$, non-dimensional exponential period

Q heat generation rate and heat input per unit volume, W/m^3

Q_0 initial exponential heat input, W/m^3

q heat flux, W/m^2

q_0 initial heat flux, W/m^2

$q_{cr,sub}$ flow transient CHF, W/m^2

$q_{cr,sub,st}$ steady-state CHF for subcooled condition, W/m^2

R_1 to R_3 resistance in a double bridge circuit, Ω

Ra average roughness, μm

$Rmax$ maximum roughness depth, μm

Rz mean roughness depth, μm

r radius, m

r_i test tube inner radius, m

r_o test tube outer radius, m

S surface area, m^2

Sc $=c_{pl}\Delta T_{sub,out}/h_{fg}$, non-dimensional outlet subcooling

Sc^* $=c_{pl}\Delta T_{sub,in}/h_{fg}$, non-dimensional inlet subcooling

T temperature of the test tube, K

$\bar{T}$ average temperature of the test tube, K

T_H homogeneous spontaneous nucleation temperature, K

T_{HET} lower limit of heterogeneous spontaneous nucleation temperature, K

T_{in} inlet liquid temperature, K

T_{out} outlet liquid temperature, K

T_s heater inner surface temperature, K

t time, s

t_d deceleration time setting, s

$\Delta T_{sub,in}$ $=(T_{sat}-T_{in})$, inlet subcooling, K

$\Delta T_{sub,in0}$ initial inlet subcooling, K

$\Delta T_{sub,out}$ $=(T_{sat}-T_{out})$, outlet subcooling, K

u inlet flow velocity, m/s

u_0 initial flow velocity, m/s

u_{cr} flow velocity at the flow transient CHF, m/s

V volume, m^3

V_I voltage drop across standard resistance, V

V_R voltage drop across two potential taps, V

V_{R1} voltage drop across two electrodes, V

V_T unbalance voltage in a double bridge circuit, V

We $=G^2d/\rho_l\sigma$, Weber number

We_{sw} $= \dfrac{G^2 d}{\rho_l \sigma} \times \left(\dfrac{\pi d^2}{\pi d^2 - 4w\delta_T} \right)^2 \times \left[\dfrac{(4y^2 + 2\pi^2)^{0.5}}{2y} \right]^2$, Weber number based on swirl velocity

w width of twisted-tape, m

y $=H/d$=(pitch of 180° rotation)/d, twist ratio of twisted-tape

α deceleration caused by a rapid decrease in velocity, (m/s^2)

δ wall thickness, mm

δ_T thickness of twisted-tape, m

λ thermal conductivity, W/mK

μ viscosity, Ns/m^2

ρ density, kg/m^3

σ surface tension, N/m

τ exponential period, s

Subscript

cr	critical
g	vapor
in	inlet
out	outlet
l	liquid
sat	saturated condition
sub	subcooled condition
wnh	with no heating

ACKNOWLEDGMENTS

This research was performed as a LHD joint research project of NIFS (National Institute for Fusion Science), Japan, NIFS13KEMF054, 2013 and 2014.

REFERENCES

[1] Gambill, W. R., Bundy, R.D., and Wansbrough, R. W., 1961, "Heat Transfer, Burnout, and Pressure Drop for Water in Swirl Flow Tubes with Internal Twisted Tapes," *Chem. Eng. Prog. Symp. Ser.*, **57** (32), pp. 127–137.

[2] Blatt, T. A., and Adt, R. R., 1963, "The Effects of Twisted Tape Swirl Generators on the Heat Transfer Rate and Pressure Drop of Boiling Freon 11 and Water," ASME-63-WA-42.

[3] Lopina, R. F., and Bergles, A.E., 1973, "Subcooled Boiling of Water in Tape Generated Swirl Flow," *J. Heat Transfer*, **95**, pp. 281–283.

[4] Celata, G. P., 1993, "Recent Achievements in the Thermal Hydraulics of High Heat Flux Components in Fusion Reactors," *Experimental Thermal and Fluid Science*, **7**, pp. 263-278.

[5] Tong, W., Bergles, A. E., and Jensen, M. K., 1996, "Critical Heat Flux and Pressure Drop of Subcooled Flow Boiling in Small-Diameter Tubes with Twisted-tape Inserts," *Journal of Enhanced Heat Transfer*, **3**, No. 2, pp. 95-108.

[6] Kabata, Y., Nakajima, R., and Shioda, K., 1996, "Enhancement of Critical Heat Flux for Subcooled Flow Boiling of Water in Tubes with a Twisted Tape and with a Helically Coiled Wire," Proc. of the ASME-JSME 4th International Conference on Nuclear Engineering, Book No. I389A2-1996, pp. 639-646.

[7] Inasaka, F., and Nariai, H., 1996, "Evaluation of subcooled critical heat flux correlations for tubes with and without internal twisted

tapes," *Nuclear Engineering and Design*, **163**, pp. 225-239.

[8] Manglik, R. M., and Bergles, A. E., 2002, Swirl Flow Heat Transfer and Pressure Drop with Twisted-Tape Inserts, Advances in Heat Transfer, **36**, Academic Press, NewYork, pp. 183–266.

[9] Bejan, A., and Kraus, A. D., 2003, Heat Transfer Handbook, John Wiley & Sons, p. 1029.

[10] Hata, K., Shirai, Y., and Masuzaki, S., 2012, "Transient Critical Heat Fluxes of Subcooled Water Flow Boiling in a Short SUS304-Tube with Twisted-Tape Insert," Proceedings of the 20th International Conference on Nuclear Engineering & ASME 2012 Power Conference ICONE20POWER2012, Paper No. ICONE20POWER2012-54212, pp. 1-13.

[11] Hata, K., Shirai, Y., and Masuzaki, S., 2013, "Transient Critical Heat Fluxes of Subcooled Water Flow Boiling in a SUS304-CIRCULAR Tube with Twisted-Tape Insert," *Journal of Power and Energy Systems*, **7**, No. 2, pp. 122-137.

[12] Hata, K., Shirai, Y., and Masuzaki, S., 2013, "Transient Critical Heat Fluxes of Subcooled Water Flow Boiling in a SUS304-Circular Tube with Various Twisted-Tape Inserts (Influence of Twist Ratio)," Proceedings of the 21st International Conference on Nuclear Engineering, July 29-August 2, 2013, Chengdu, China, Paper No. ICONE21-15323, pp. 1-13.

[13] Hata, K., Fukuda, K., and Masuzaki, S., 2014, "Transient Critical Heat Fluxes of Subcooled Water Flow Boiling in a SUS304-Circular Tube with Various Twisted-Tape Inserts (Influence of Twist Ratio)," *Journal of Thermal Science and Engineering Applications*, Trans. ASME, **6**, pp. 031010-1-14.

[14] Hata, K., and Masuzaki, S., 2011, "Subcooled Water Flow Boiling Heat Transfer in a Short SUS304-Tube with Twisted-Tape Insert," *Journal of Engineering for Gas Turbines and Power*, Trans. ASME, **133**, pp. 052906-1-11.

[15] Hata, K., and Masuzaki, S., 2011, "Heat Transfer and Critical Heat Flux of Subcooled Water Flow Boiling in a SUS304-Tube with Twisted-Tape Insert," *Journal of Thermal Science and Engineering Applications*, Trans. ASME, **3**, pp. 012001-1-12.

[16] Hata, K., and Masuzaki, S., 2011, "Twisted-Tape- Induced Swirl Flow Heat Transfer and Pressure Drop in a Short Circular Tube under Velocities Controlled," *Nuclear Engineering and Design*, **241**, pp. 4434-4444.

[17] Hata, K., and Noda, N., 2008, "Transient Critical Heat Fluxes of Subcooled Water Flow Boiling in a Short Vertical Tube Caused by Exponentially Increasing Heat Inputs," *Journal of Heat Transfer*, Trans. ASME, Series C, **130**, pp. 054503-1-9.

[18] Hata, K., and Masuzaki, S., 2010, "Influence of Heat Input Waveform on Transient Critical Heat Flux of Subcooled Water Flow Boiling in a Short Vertical Tube," *Nuclear Engineering and Design*, **240**, pp. 440-452.

[19] Spalding, D. B., 1991, *The PHOENICS Beginner's Guide*, CHAM Ltd., London, United Kingdom.

[20] Brodkey, R. S., and Hershey, H. C., 1988, *Transport Phenomena*, McGraw-Hill, New York, p. 568.

[21] Hata, K., Shirai, Y., and Masuzaki, S., 2013, "Heat Transfer and Critical Heat Flux of Subcooled Water Flow Boiling in a

Horizontal Circular Tube," *Experimental Thermal and Fluid Science*, **44**, pp. 844-857.

[22] Hata, K., Shiotsu, M., and Noda, N., 2004, "Critical Heat Fluxes of Subcooled Water Flow Boiling against Outlet Subcooling in Short Vertical Tube," *Journal of Heat Transfer*, Trans. ASME, Series C, **126**, pp. 312-320.

[23] Hata, K., Komori, H., Shiotsu, M., and Noda, N., 2004, "Critical Heat Fluxes of Subcooled Water Flow Boiling against Inlet Subcooling in Short Vertical Tube," *JSME International Journal*, Series B, **47**, No. 2, pp. 306-315.

[24] Hata, K., Shiotsu, M., and Noda, N., 2006, "Critical Heat Flux of Subcooled Water Flow Boiling for High *L/d* Region," *Nuclear Science and Engineering*, **154**, No. 1, pp. 94-109.

[25] Hata, K., Shiotsu, M., and Noda, N., 2006, "Influence of Heating Rate on Subcooled Flow Boiling Critical Heat Flux in a Short Vertical Tube," *JSME International Journal*, Series B, **49**, No. 2, pp. 309-317.

[26] Hata, K., Shiotsu, M., and Noda, N., 2007, "Influence of Test Tube Material on Subcooled Flow Boiling Critical Heat Flux in Short Vertical Tube," *Journal of Power and Energy Systems*, **1**, No. 1, pp. 49-63.

[27] Hata, K., and Noda, N., 2008, "Turbulent Heat Transfer for Heating of Water in a Short Vertical Tube," *Journal of Power and Energy Systems*, **2**, No. 1, pp. 318-329.

[28] Hata, K., and Noda, N., 2008, "Transient Critical Heat Fluxes of Subcooled Water Flow Boiling in a Short Vertical Tube Caused by Exponentially Increasing Heat Inputs," *Journal of Heat Transfer*, Trans. ASME, Series C, **130**, pp. 054503-1-9.

[29] Hata, K., and Masuzaki, S., 2009, "Subcooled Boiling Heat Transfer in a Short Vertical SUS304-Tube at Liquid Reynolds Number Range 5.19×10^4 to 7.43×10^5," *Nuclear Engineering and Design*, **239**, pp. 2885-2907.

[30] Hata, K., and Masuzaki, S., 2010, "Subcooled Boiling Heat Transfer for Turbulent Flow of Water in a Short Vertical Tube," *Journal of Heat Transfer*, Trans. ASME, Series C, **132**, pp. 011501-1-11.

[31] Hata, K., and Masuzaki, S., 2010, "Influence of Heat Input Waveform on Transient Critical Heat Flux of Subcooled Water Flow Boiling in a Short Vertical Tube," *Nuclear Engineering and Design*, **240**, pp. 440-452.

[32] Hata, K., and Masuzaki, S., 2010, "Critical Heat Fluxes of Subcooled Water Flow Boiling in a Short Vertical Tube at High Liquid Reynolds Number," *Nuclear Engineering and Design*, **240**, pp. 3145-3157.

[33] Kutateladze, S.S., 1959, "Heat Transfer in Condensation and Boiling," AEC-tr-3770, USAEC.

[34] Zuber, N., 1959, "Hydrodynamic Aspects of Boiling Heat Transfer," AECU-4439, USAEC.

[35] Cole, C., 1979, "Homogeneous and heterogeneous nucleation in Boiling Phenomena," Vol. 1, Stralen, S. van, and Cole, R. eds., Hemisphere Pub. Corp., p. 71.

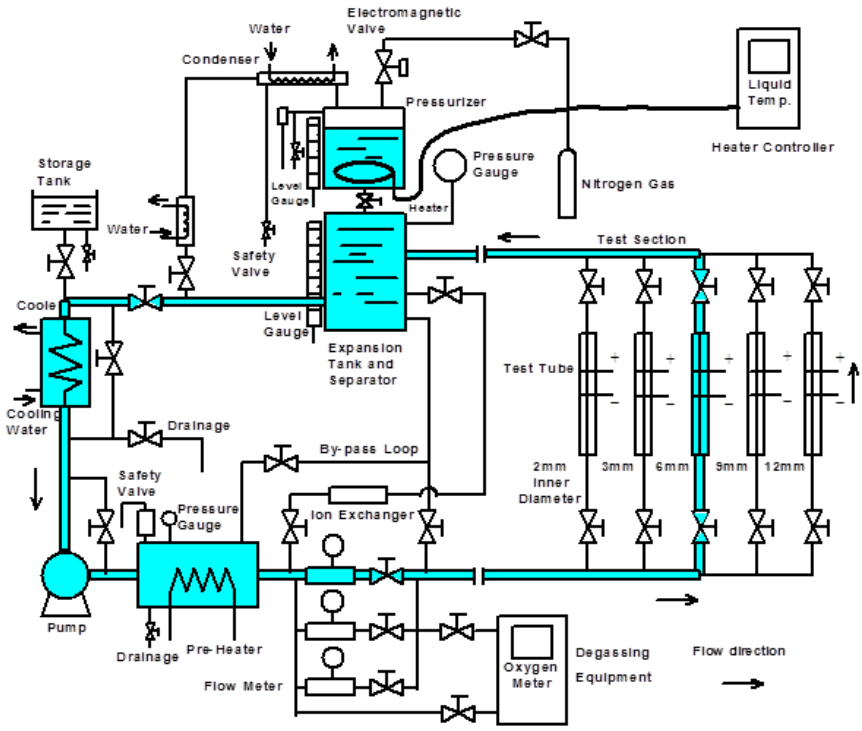

Fig. 1 Schematic diagram of experimental water loop

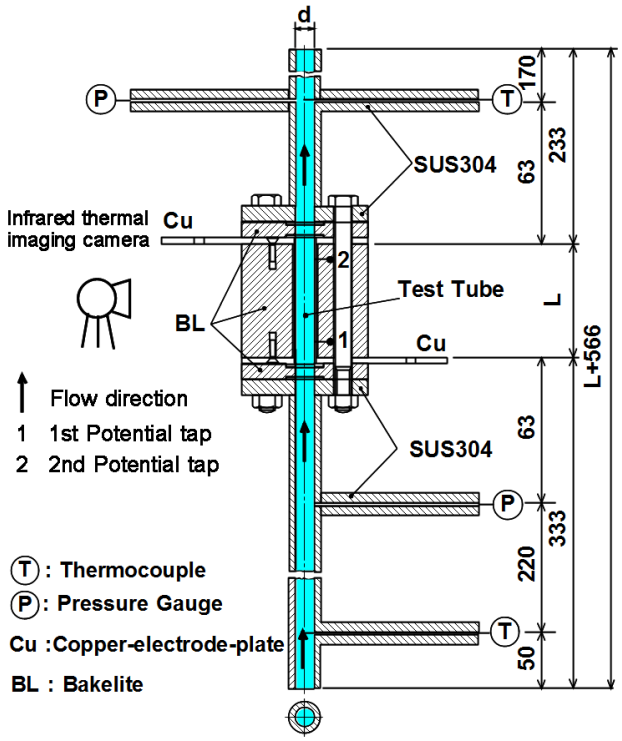

Fig. 2 Vertical cross-sectional view of 6 mm inner diameter test section

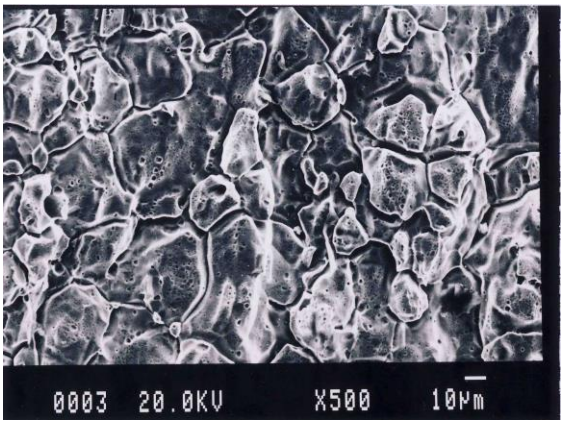

Fig. 3 SEM photograph for the SUS304 test tube of *d*=6 mm with the rough finished inner surface

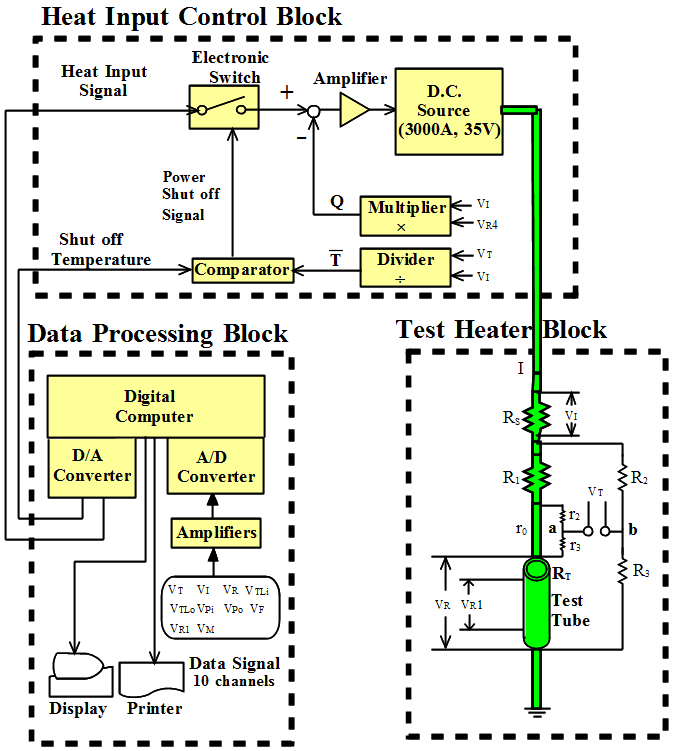

Fig. 4 Measurement and data processing system

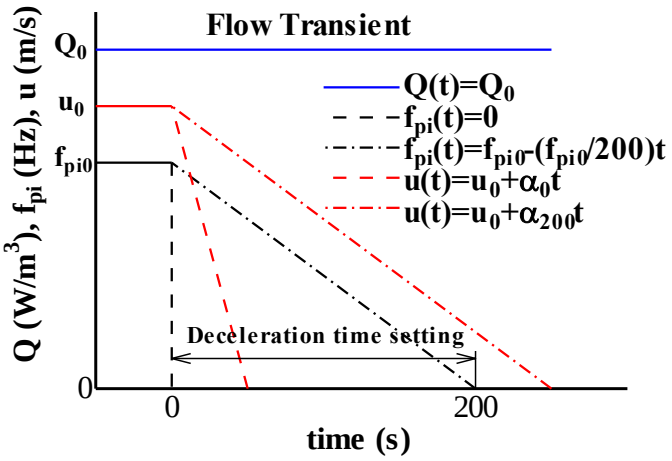

Fig. 5 Time variations in pump input frequency and flow velocity for flow transient CHF experiment

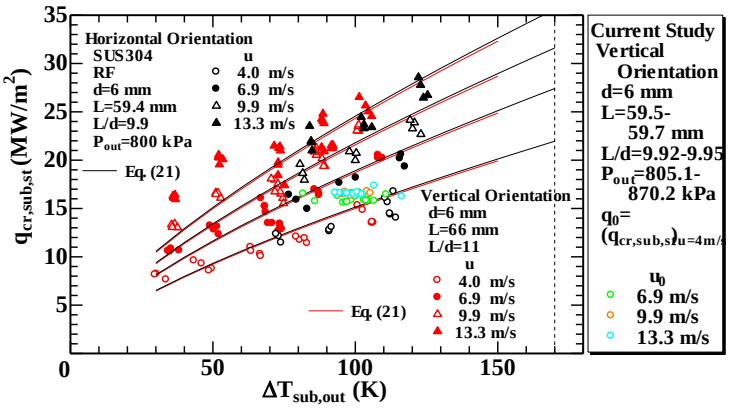

Fig. 6 $q_{cr,sub,st}$ vs. $\Delta T_{sub,out}$ for an inner diameter of 6mm with the heated length of 59.5 to 59.7 mm at outlet pressures of 805.1 to 870.2 kPa

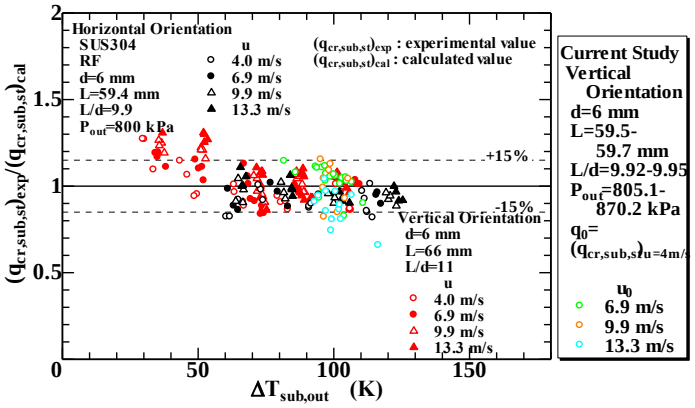

Fig. 7 Ratios of CHF data for the inner diameter of 6 mm to the values derived from the outlet CHF correlation, Eq. (21), versus $\Delta T_{sub,out}$ at outlet pressures of 805.1 to 870.2 kPa

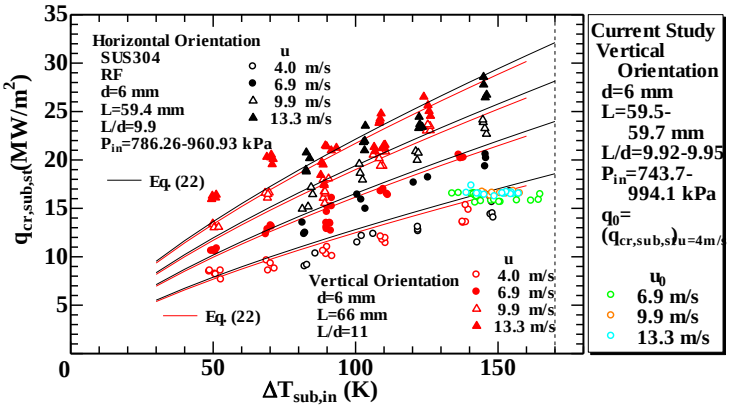

Fig. 8 $q_{cr,sub,st}$ vs. $\Delta T_{sub,in}$ for an inner diameter of 6mm with the heated length of 59.5 to 59.7 mm at inlet pressures of 743.7 to 994.1 kPa

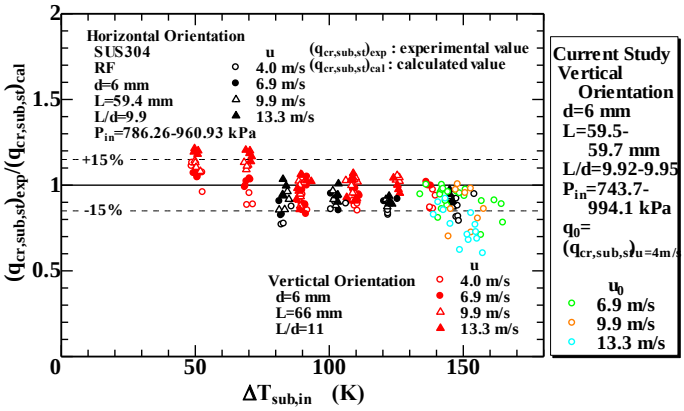

Fig. 9 Ratios of CHF data for the inner diameter of 6 mm to the values derived from the inlet CHF correlation, Eq. (22), versus $\Delta T_{sub,in}$ at inlet pressures of 743.7 to 994.1 kPa

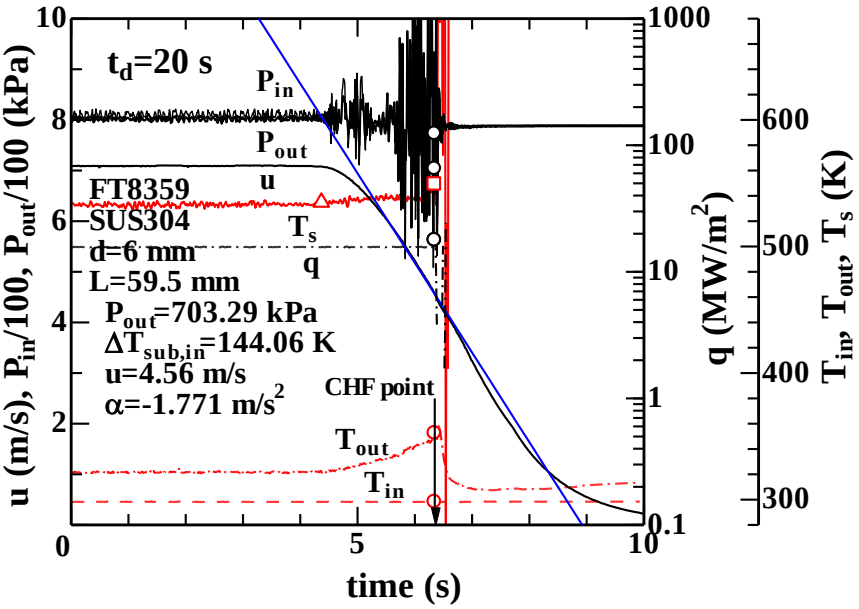

Fig. 10 Time variations in P_{in}, P_{out}, T_{in}, T_{out}, T_s, q and u for u_0=7.09 m/s, q_0=15.73 MW/m^2 and α=-1.771 m/s^2 at P_{out0}=801.37 kPa and $\Delta T_{sub,in0}$=145.83 K

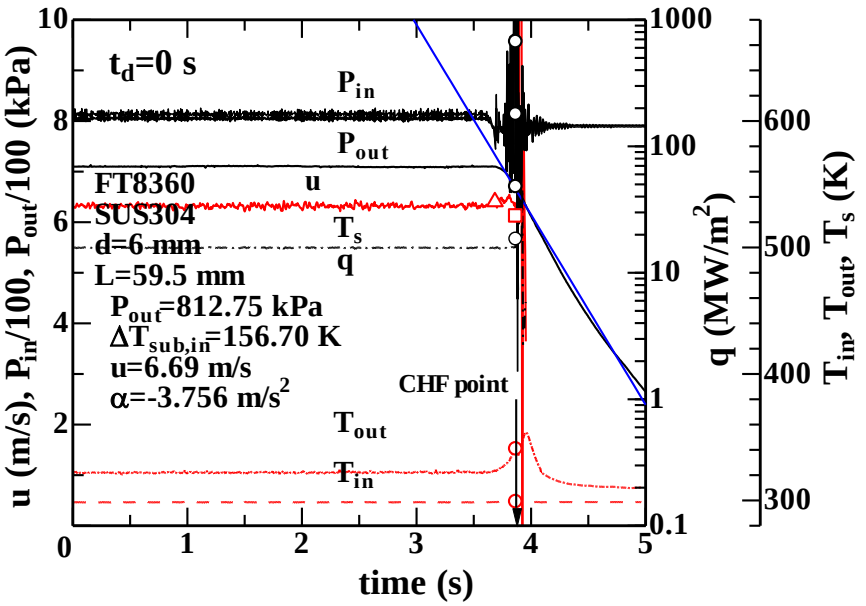

Fig. 11 Time variations in P_{in}, P_{out}, T_{in}, T_{out}, T_s, q and u for u_0=7.10 m/s, q_0=15.81 MW/m^2 and α=-3.756 m/s^2 at P_{out0}=805.19 kPa and $\Delta T_{sub,in0}$=145.69 K

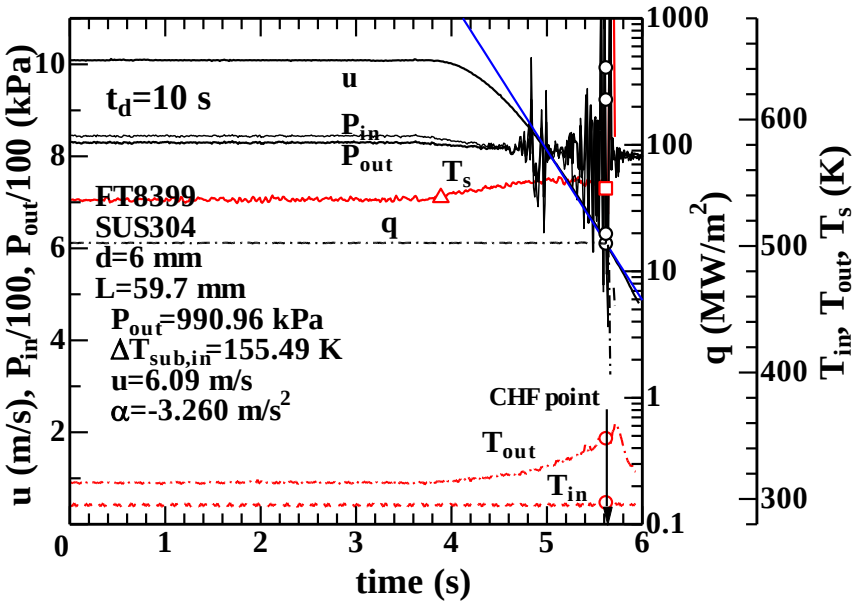

Fig. 12 Time variations in P_{in}, P_{out}, T_{in}, T_{out}, T_s, q and u for u_0=10.09 m/s, q_0=16.78 MW/m^2 and α=-3.260 m/s^2 at P_{out0}=829.89 kPa and $\Delta T_{sub,in0}$=150.56 K

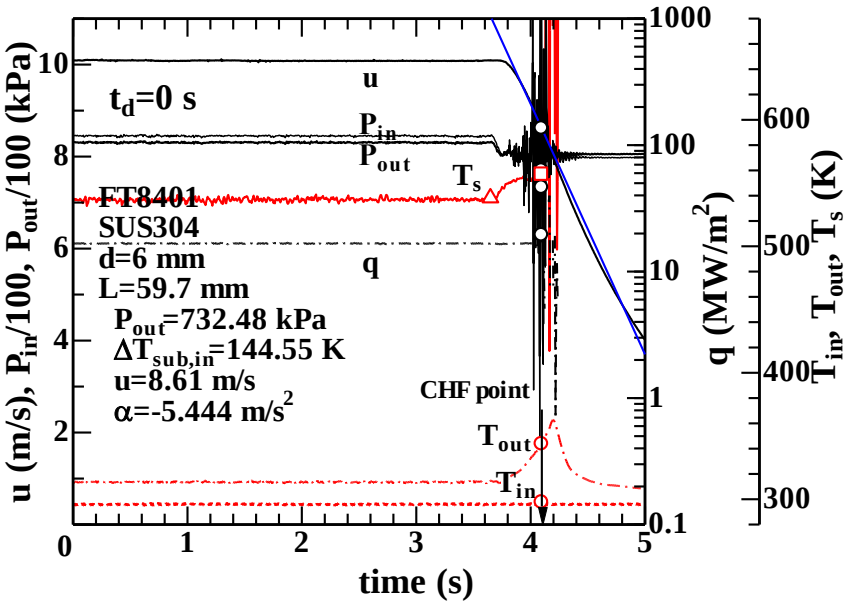

Fig. 13 Time variations in P_{in}, P_{out}, T_{in}, T_{out}, T_s, q and u for, u_0=10.08 m/s, q_0=16.70 MW/m^2 and α=-5.444 m/s^2 at P_{out0}=830.62 kPa and $\Delta T_{sub,in0}$=149.85 K

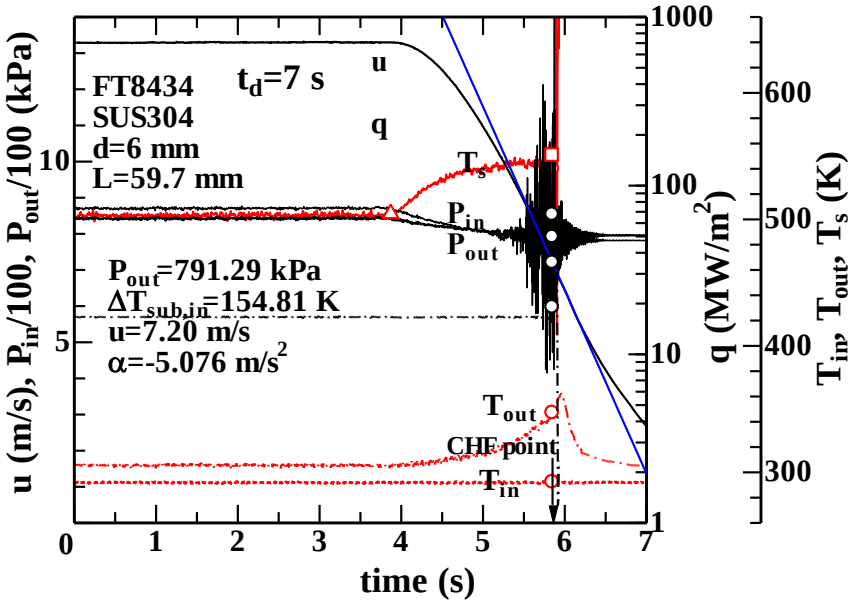

Fig. 14 Time variations in P_{in}, P_{out}, T_{in}, T_{out}, T_s, q and u for u_0=13.30 m/s, q_0=16.62 MW/m^2 and α=-5.076 m/s^2 at P_{out0}=842.63 kPa and $\Delta T_{sub,in0}$=155.21 K

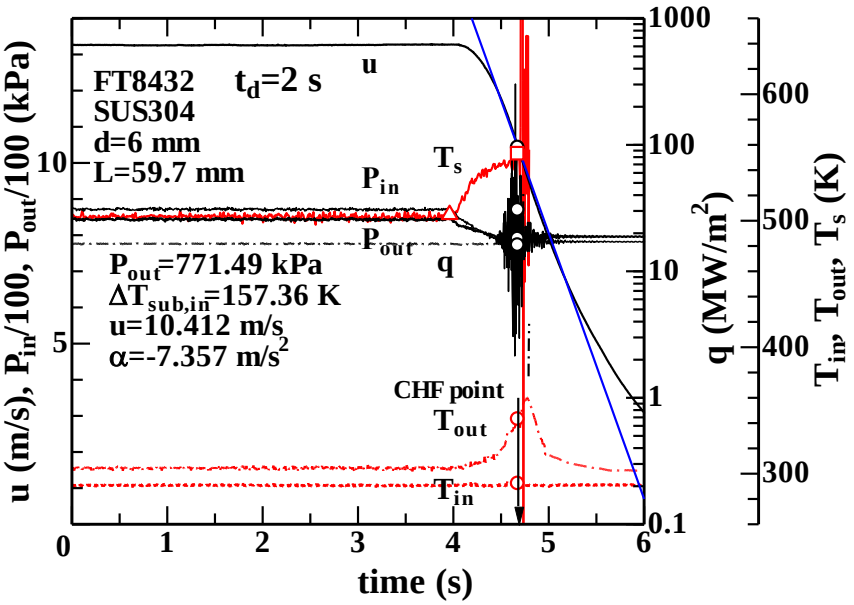

Fig. 15 Time variations in P_{in}, P_{out}, T_{in}, T_{out}, T_s, q and u for u_0=13.26 m/s, q_0=16.51 MW/m^2 and α=-7.357 m/s^2 at P_{out0}=843.60 kPa and $\Delta T_{sub,in0}$=156.32 K

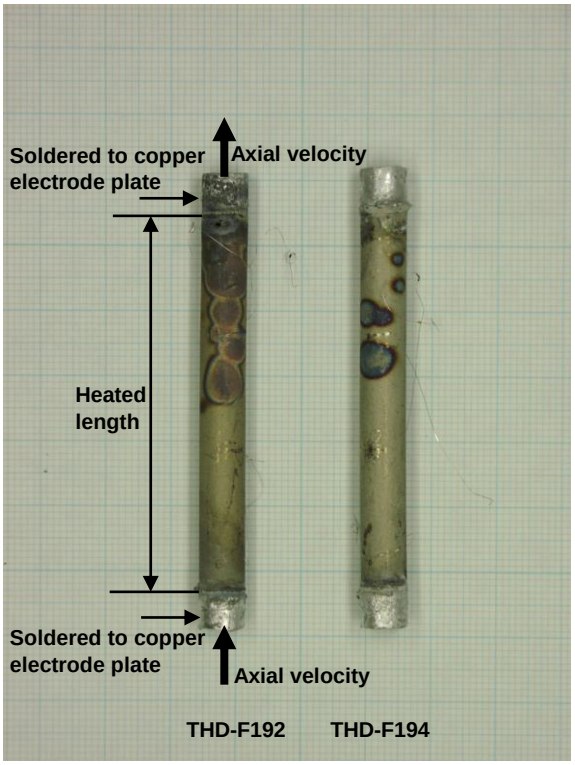

Fig. 16 Typical photograph for SUS304 test tubes of d=6 mm and L=59.7 mm burned out in flow transient CHF experiments

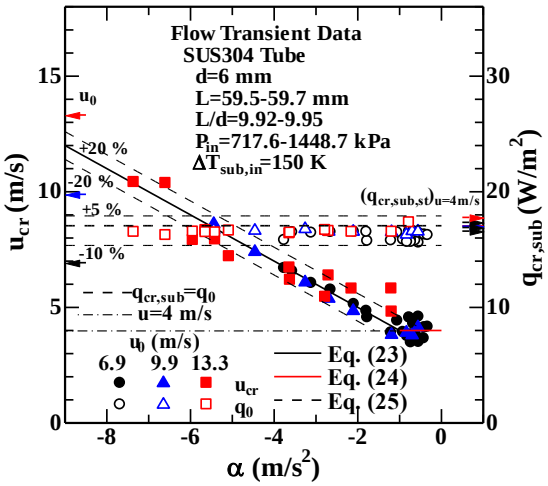

Fig. 17 Relationship between u_{cr} and α and that between $q_{cr,sub}$ and α with u_0=6.9, 9.9 and 13.3 m/s at $q_0=(q_{cr,sub,st})_{u=4m/s}$ W/m^2 for P_{out}=800 kPa and T_{in}=290.12 to 308.51 K

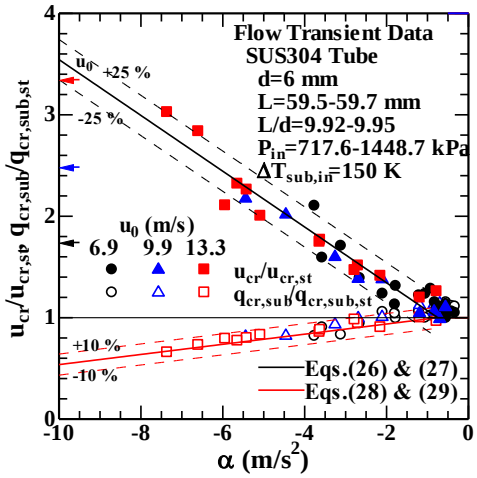

Fig. 18 Relationship between $u_{cr}/u_{cr,sub,st}$ and α and that between $q_{cr}/q_{cr,sub,st}$ and α with u_0=6.9, 9.9 and 13.3 m/s at $q_0=(q_{cr,sub,st})_{u=4m/s}$ W/m^2 for P_{out}=800 kPa and T_{in}=290.12 to 308.51 K

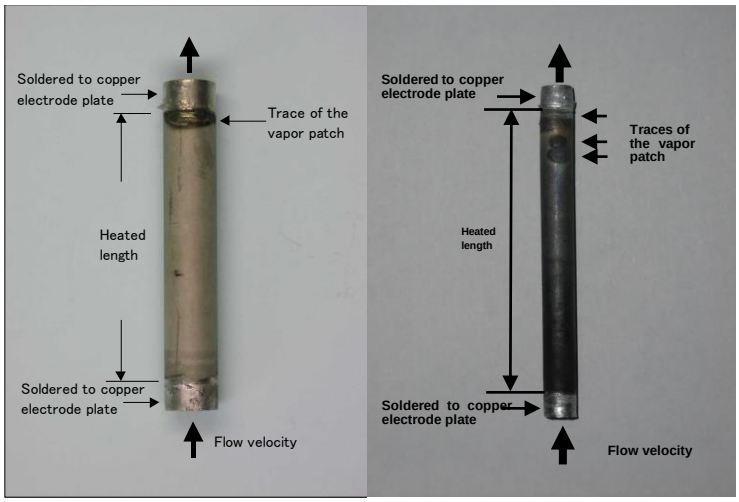

(a) (b)

Fig. 19 Typical photograph of the used test tubes with (a) d=9 mm and L=48 mm [22], and (b) d=6 mm and L=59.5 mm [31, 32] burned out due to the hydrodynamic instability

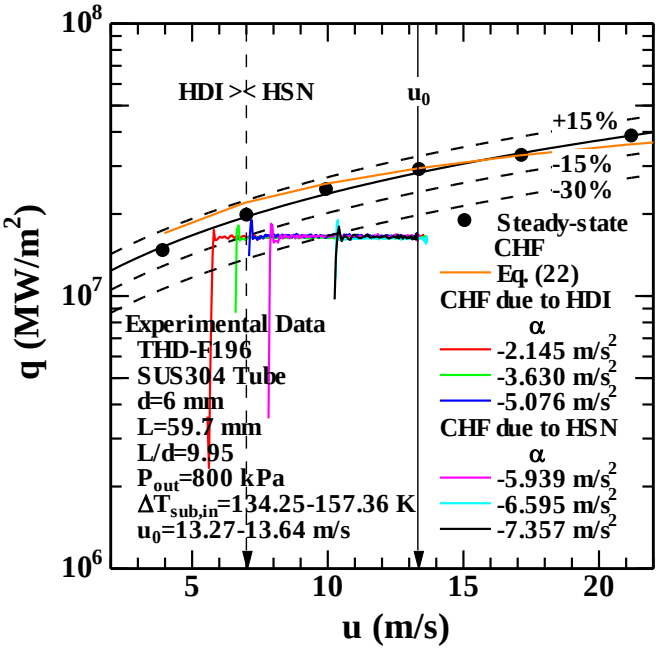

Fig. 20 Transient boiling heat transfer processes on q versus u with various decelerations caused by a rapid decrease in velocity α=-2.15, -3.63, -5.08, -5.94, -6.60 and -7.36 m/s^2 from u_0=13.3 m/s for d=6 mm